The Astrophysical Journal, 674:80–96, 2008 February 10

EVIDENCE FOR QUASAR ACTIVITY TRIGGERED BY GALAXY MERGERS IN *HST* OBSERVATIONS OF DUST-REDDENED QUASARS

Tanya Urrutia,[1,2] Mark Lacy,[3] and Robert H. Becker[1,2]

Received 2007 May 23; accepted 2007 September 15

ABSTRACT

We present *Hubble Space Telescope* ACS images of 13 dust-reddened type 1 quasars selected from the FIRST/2MASS Red Quasar Survey. These quasars have high intrinsic luminosities after correction for dust obscuration ($-23.5 \geq M_B \geq -26.2$ from K-magnitude). The images show strong evidence of recent or ongoing interaction in 11 of the 13 cases, even before the quasar nucleus is subtracted. None of the host galaxies are well fit by a simple elliptical profile. The fraction of quasars showing interaction is significantly higher than the 30% seen in samples of host galaxies of normal, unobscured quasars. There is a weak correlation between the amount of dust reddening and the magnitude of interaction in the host galaxy, measured using the Gini coefficient and the concentration index. Although few host galaxy studies of normal quasars are matched to ours in intrinsic quasar luminosity, no evidence has been found for a strong dependence of merger activity on host luminosity in samples of the host galaxies of normal quasars. We thus believe that the high merger fraction in our sample is related to their obscured nature, with a significant amount of reddening occurring in the host galaxy. The red quasar phenomenon seems to have an evolutionary explanation, with the young quasar spending the early part of its lifetime enshrouded in an interacting galaxy. This might be further indication of a link between AGNs and starburst galaxies.

Subject headings: galaxies: active — galaxies: evolution — galaxies: interactions — quasars: general

Online material: color figures

1. INTRODUCTION

The existence of a link between AGNs and starbursts/ultraluminous infrared galaxies (ULIRGs) in the local universe has been discussed for a long time (e.g., Heckman et al. 1989; Sanders & Mirabel 1996; Cid Fernandes et al. 2001). Further evidence for such a link comes from the tight correlation between nuclear black hole mass and bulge mass (e.g., Magorrian et al. 1998; Tremaine et al. 2002) and the black hole mass-host galaxy velocity dispersion (M-σ) relation in local galaxies (e.g., Ferrarese & Merritt 2000; Gebhardt et al. 2000), which suggest that star-formation and accretion onto black holes in galaxies are intimately connected. However, *Hubble Space Telescope* (*HST*) imaging of the host galaxies of luminous quasars to moderate depths showed that most of them have the morphology of elliptical galaxies, with little evidence for ongoing star formation (Dunlop et al. 2003). At low redshift only 30% of the host galaxies show obvious signs of disturbance (Guyon et al. 2006). Although quasars with infrared excesses are thought to host starbursts (Canalizo & Stockton 2001), these are a small minority of the optically selected quasar population.

Recent surveys have shown that optically selected quasars comprise less than half of the total quasar population (Martínez-Sansigre et al. 2005; Stern et al. 2005). Optical quasar surveys tend to miss dust-reddened quasars which have been found either with infrared surveys (Cutri et al. 2001; Lacy et al. 2004), radio surveys (White et al. 2003), hard X-ray surveys (Norman et al. 2002), or surveys for high-ionization narrow-line objects (Zakamska et al. 2006). Therefore they represent a new and largely uninvestigated quasar population, which may have many members that are at an earlier stage in their quasar activity in which dust and gas debris from the merger block the view of the central AGN. This fits with population synthesis models of the X-ray background that predict that a large fraction (close to 80%) of the accretion process in AGNs is obscured and only the most energetic photons (>20 keV) can penetrate the obscuring dust barrier (Gilli et al. 2001, 2007; Ueda et al. 2003).

Dusty quasars are generally divided into type 2 quasars, which show only narrow-line emission in the rest-frame optical, and have inferred extinctions toward the nucleus of $A_V \sim 5$–100, and lightly dust-reddened type 1 quasars, which still show broad lines and quasar continua in the optical, but have significant reddening relative to a normal quasars ($A_V \sim 1$–5).

Surveys in the mid-infrared have been able to make approximate census of the obscured quasar population. Brown et al. (2006) and Lacy et al. (2007) find that the fraction of lightly dust-reddened type 1 quasars is between 20% and 30% of the total type-1 population. Lacy et al. (2007) also shows that the type-1 population (unreddened plus lightly reddened) is about 50% of the total quasar population, the remainder being type 2.

The nature of both populations remains uncertain. At present, there are two competing models to explain the obscuration in dusty quasars: orientation vs. evolution. In the orientation model, dust-reddened quasars are observed side-on to a disk or torus of obscuring material (e.g., Antonucci 1993), whereas in the evolution model, dusty quasars are viewed as an early stage in the life of a quasar, where the nucleus is obscured by debris from a merger and starburst which triggers the nuclear activity, prior to quasar winds expelling the dust (e.g., Sanders et al. 1989). Of particular interest are the class of lightly reddened quasars, where the reddening is smaller than that expected from a torus seen edge-on. These objects are good candidates for reddening by dust in the host galaxy, but may also correspond to objects in which the line of sight grazes the edge of the torus.

Recent simulations of galaxy mergers tend to support the evolution model, and suggest that the active nucleus is obscured for a

[1] Department of Physics, University of California, One Shields Avenue, Davis, CA 95616; urrutia@physics.ucdavis.edu.

[2] IGPP, L-413, Lawrence Livermore National Laboratory, Livermore, CA 94550; bob@igpp.ucllnl.org.

[3] *Spitzer* Science Center, MS 314-6, California Institute of Technology, 1200 East California Boulevard, Pasadena, CA 91125; mlacy@ipac.caltech.edu.

long time before the feedback from the accretion disperses the obscuring material (Hopkins et al. 2005). In this picture, the quasar is seen in the optical regime only at the end of its lifetime, when it is the most luminous, radiating close to the Eddington limit and therefore being capable of expelling the dust (Hopkins et al. 2006). A large population of these young, obscured, underluminous quasars would also account for the mostly hard X-ray background; however, there is still debate on the normalization factor of the hard X-ray background, that is the fraction of these sources is still unknown. Observations of type 2 quasars discovered in the Sloan Digital Sky Survey (SDSS), however, tend to support the orientation hypothesis, with broad lines seen in polarized light, and host galaxies consistent with those of normal type-1 quasars (Zakamska et al. 2006). Similarly, an *HST* study of lightly-reddened type-1 quasars selected from 2MASS found no significant difference in the properties of host galaxies of infrared selected quasars from quasars selected from other methods (Marble et al. 2003), although ground-based studies of a similar sample found more signs of interactions (Hutchings et al. 2003, 2006).

This paper focuses on *HST* observations of a sample of lightly dust-reddened type-1 quasars with $0.4 < z < 1$, selected using a combination of the FIRST radio survey and the 2MASS infrared survey. The primary objective is to study the host galaxies of red quasars and to assess if their morphologies show signs of recent interactions. We adopt a flat universe, $H_0 = 70$ km s^{-1} Mpc^{-1}, $\Omega_\Lambda = 0.7$ cosmology.

2. BACKGROUND AND SAMPLE SELECTION

2.1. *The F2M Sample*

We have selected a sample of luminous, dust-reddened quasars using a combination of 2MASS infrared survey (Skrutskie et al. 1995) and the FIRST radio survey (Becker et al. 1995) in order to answer some of the questions posed above. The bulk of these dust-reddened type 1 quasars have reddenings around $E(B-V) \lesssim 1.5$, which makes them much more heavily reddened than other red quasar samples (Cutri et al. 2001; Richards et al. 2003), but they do not show the amount of obscuration as true type-2 quasars. The methodology and preliminary results of this sample are described in Glikman et al. (2004) and the final results in Glikman et al. (2007). We have used two different color selection techniques, both of which seem to be highly effective at finding red quasars ($J-K > 1.7$ and $R-K > 4$; or $R-K > 5$). We have followed up our candidates with Keck (ESI) and IRTF (Spex) to obtain spectra in the optical and near-infrared. Some of these objects show only narrow lines in the observed-frame optical, but spectroscopy of the quasars in the near-IR have show very broad Hα or Paschen lines. So far, about 100 red quasars have been found with this method, which would have been missed by traditional optical quasar surveys (Glikman et al. 2007). Following their conventions, objects from the FIRST-2MASS red quasars survey are named F2M.

In contrast to the 2MASS quasar sample of Marble et al. (2003), which were mostly low redshift, low luminosity, and selected by their near-infrared colors alone, the red quasars in our FIRST/2MASS study have a median redshift of 0.7. We therefore expect the F2M sample to have higher luminosity and perhaps more star formation in the host galaxies than other red quasar samples at lower redshift.

While the selection of red quasars based on $R-K$ colors could include objects which are red due to galaxy starlight in the infrared, the objects in this sample are intrinsic high-luminosity quasars, in which the galaxy light should add a negligible contribution in the K band. This becomes evident when we measure the reddening of the quasars.

2.2. *Sample Spectra*

From the F2M sample, we chose a subsample of 13 $0.4 < z < 1.0$ red quasars to image to inspect their host galaxy properties. In this section we will describe their optical spectra, taken mostly with ESI on Keck.

We fit the optical red quasar spectra to a model of an unreddened quasar. For that we use the FBQS composite spectrum (Brotherton et al. 2001) with a SMC dust-reddening law from Fitzpatrick (1999) using the relation

$$F_o(\lambda) = F_c(\lambda) \times 10^{E(B-V)k(\lambda)}, \quad (1)$$

with $F_c(\lambda)$ the composite (FBQS) and $F_o(\lambda)$ the observed spectrum. Typically the SMC extinction curve $k(\lambda)$ lacks a significant 2175 Å bump seen in Galactic dust. We follow the conventions from Fitzpatrick & Massa (1990) to obtain the extinction curve $k(\lambda)$, with $R_V = 3.1$ (Galactic value).

Figure 1 shows the spectra of our quasars. The black line is the observed spectrum, the dotted line is the FBQS composite redshifted and normalized to the quasar flux and the thick gray line is the FBQS composite with the deduced reddening correction applied. The derived $E(B-V)$ values are shown in Table 1; the values have such high errors in $E(B-V)$ either because there was low signal-to-noise in the spectrum or because the rms of the fit was not very good. Because there can be significant host galaxy contribution to the optical spectra, especially in the UV, our $E(B-V)$ estimates can serve as a lower limit. Glikman et al. (2007) also includes the near-infrared SPEX spectra to their fitting, so in some cases there is some discrepancy between their quoted values and ours. Their deduction of the reddening is beyond the scope of this paper, so we will only take the optical spectrum for an estimate of the reddening of the total system.

For most of the quasars the reddening fits are consistent with dust-reddening and very little red starlight from the host galaxy is required. However, this is not the case for F2M0825+4716, F2M0915+2418, and F2M1151+5359 in which the fit for $E(B-V)$ broke down. These objects will be important later when we inspect the properties of their host galaxies. Note also that the reddenings are significant enough that the red colors of the quasars could not solely have come from a "red" spectral slope. Even though the F2M sample is radio selected, the radio fluxes of the objects (Table 1) are also weak; the quasars are radio intermediate at best, so a strong synchrotron component showing up in the infrared is unlikely to have much contribution to the red color.

Once we have the reddening $E(B-V)$, we can also derive the intrinsic luminosities of the F2M quasars from the spectrum (corrected for obscuration). We also calculated the luminosities of the quasars from the K-band magnitude assuming that in the K band there is no host galaxy contribution. The range between the absolute magnitude derived from the spectrum and from the K-band magnitude sometimes is quite large implying either that there were some large slit losses or that even in the K band there is significant host galaxy contribution, see Table 1. We are more inclined to use the derived luminosity from the K band, since the slit will miss the obscured AGN often and as mentioned before, the $E(B-V)$ values are only a lower limit as there is host galaxy contribution to the spectrum and we do not have the full wavelength coverage ranging into the mid-infrared to get the true continuum shape. The fact that the K-band magnitude is so bright implies that the reddenings must be larger. What we can say is that the quasars are more luminous than usual, having

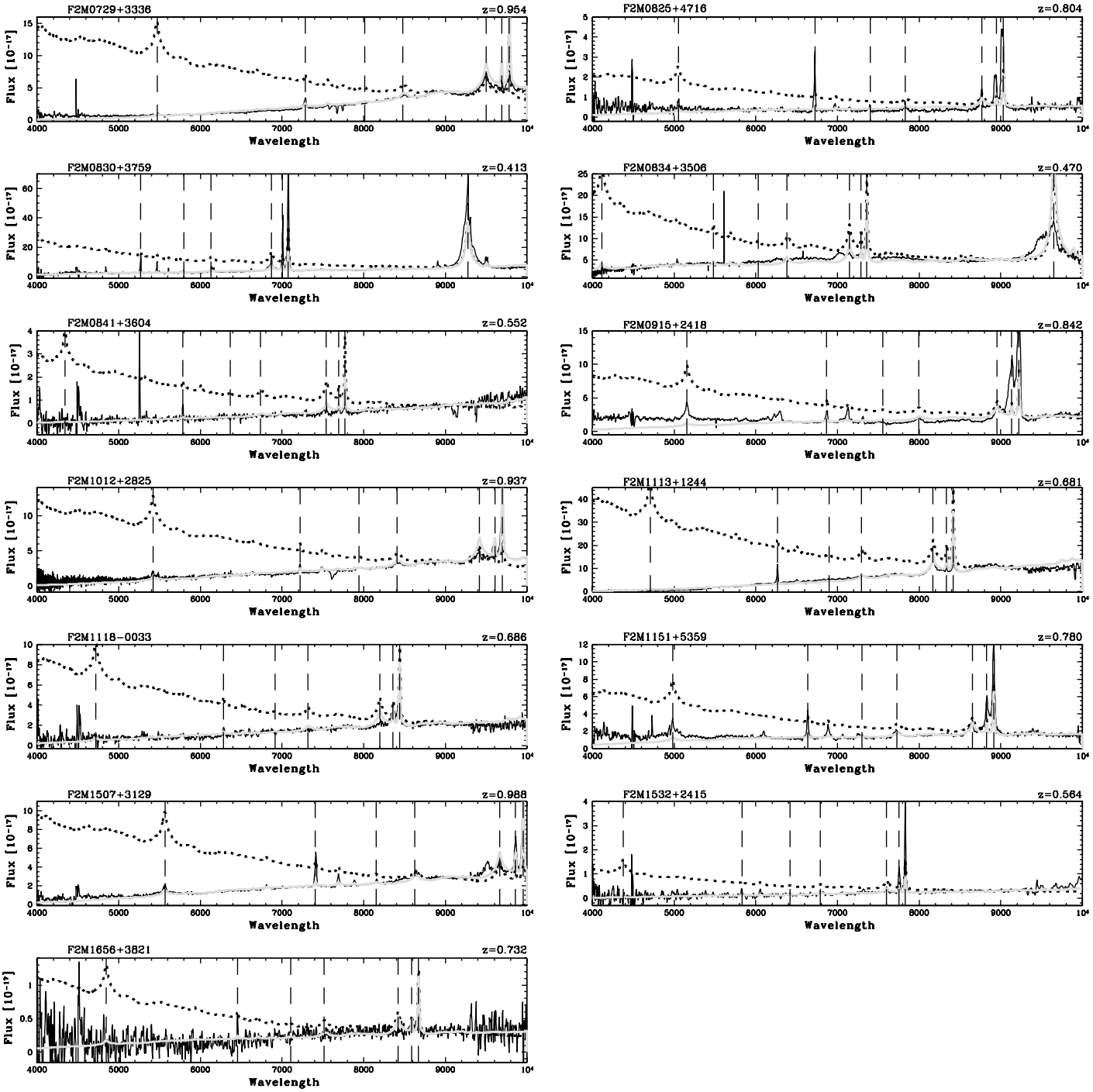

FIG. 1.—Spectra of the FIRST/2MASS red quasars observed with *HST*. The black line in the quasar spectrum, the dotted line the FBQS quasar composite redshifted to the quasar's redshift and the thick gray line after applying a SMC reddening law to the FBQS composite. [*See the electronic edition of the Journal for a color version of this figure.*]

a luminosity range of $-23.5 \geq M_B \geq -26.2$ derived from the K-band magnitude. Typical quasar luminosity functions at similar redshifts as our sample have only the highest luminosity quasars above $M_B \sim -24.5$ (our mean value), with a steepening of the function at around $M_B \sim -23.5$ for quasars at a redshift of $z \sim 0.7$ (e.g., Hopkins et al. 2007b). The high values of M_B we find for our quasars suggests that we are missing the majority of this type of objects. Thus, because of the shallowness of the 2MASS survey we are only able to probe the tip of the "red quasar iceberg."

3. *HST* ACS OBSERVATIONS

We followed up this subsample of 13 F2M red quasars with the ACS Wide Field Camera on *HST* (GO-10412). They were imaged with the F475W and the F814W filters, which roughly correspond to g' and I_C filters. The redshift range was chosen such that all our objects had their intrinsic luminosities well above the quasar/Seyfert divide (so that the near-IR magnitudes used in their selection would not have much contribution from the host galaxies), and all were at low enough redshift that emission above rest-frame 4000 Å fell within the bandpass of the F814W filter on ACS. The observing dates and corresponding exposure times are presented in Table 2.

Most of the objects were observed for one *HST* orbit. However, as the sample of red quasars spanned a significant range of redshift, two high-redshift quasars ($z > 0.9$) were observed for two orbits each to ensure a more uniform surface brightness limit

TABLE 1
Source Properties

Source	z	K Magnitude	Radio Flux 1.4 GHz (mJy)	$E(B-V)$ (rest)	Luminosity Spectrum/K Magnitude
F2M0729+3336.....	0.954	14.5	3.3	0.83 ± 0.22	−25.0/−25.6
F2M0825+4716.....	0.804	14.1	61.1	0.50 ± 0.35	−21.9/−25.8
F2M0830+3759.....	0.413	14.6	6.4	0.80 ± 0.15	−22.7/−23.5
F2M0834+3506.....	0.470	14.7	1.2	0.53 ± 0.10	−22.9/−23.7
F2M0841+3604.....	0.552	14.9	6.5	1.05 ± 0.64	−21.0/−23.9
F2M0915+2418.....	0.842	13.8	9.8	0.53 ± 0.36	−23.7/−26.2
F2M1012+2825.....	0.937	15.2	9.2	0.66 ± 0.12	−24.4/−25.0
F2M1113+1244.....	0.681	13.7	3.0	1.01 ± 0.24	−25.1/−25.5
F2M1118−0033.....	0.686	14.6	1.3	0.72 ± 0.26	−23.0/−24.6
F2M1151+5359.....	0.780	15.1	3.5	0.47 ± 0.13	−23.3/−24.7
F2M1507+3129.....	0.988	15.1	7.8	0.54 ± 0.13	−24.3/−24.8
F2M1532+2415.....	0.564	15.0	7.4	0.90 ± 0.53	−20.5/−23.9
F2M1656+3821.....	0.732	15.1	4.1	0.55 ± 0.57	−20.9/−24.5

for the sample as a whole. These images were drizzled with the python program `multidrizzle` in the usual manner. For the images with only one orbit we used the readily available drizzled products from the archive, since they did not have significant cosmic-ray contamination.

Color composite images of the red quasars are shown in Figure 2. Inspecting the images by eye, one can see much more information of the host galaxy than one would from a blue quasar in which the quasar light dominates. However, the images reveal much more interaction than the usual fraction of 30% (Marble et al. 2003; Guyon et al. 2006) with tidal tails and many irregularities present in the host galaxies.

Some of the images show several compact knots or nuclei. If the merger was driven by two galaxies with central black holes, it is possible that the two of them ignite as AGNs, before merging into a massive active galaxy with only one black hole in the center. This has been observed in NGC 6240, an ultraluminous infrared galaxy at very low redshift (Komossa et al. 2003). Table 3 summarizes the properties of the quasars that show more than one candidate nucleus. F2M0841+3604, which has the largest angular separation, was observed with *Chandra*, but only had seven (very hard) counts, which is not enough to resolve both components. Two of the objects also have double-peaked broad lines, F2M0825+4716 and F2M1507+3129. Such emission lines are not uncommon in broad-line radio galaxies, and are thought to be due to a disklike broad-line region seen edge-on (e.g., Eracleous & Halpern 1994), however, they could also be from two separate active nuclei close to merger. Unfortunately, neither of these show multiple nuclei in their images.

TABLE 2
Journal of *HST* Observations

Source	Observation Date	Exposure Time (s) Red	Exposure Time (s) Blue
F2M0729+3336.....	2005 Oct 24	4650	4760
F2M0825+4716.....	2005 Oct 19	1820	1924
F2M0830+3759.....	2005 Apr 18	1720	1832
F2M0834+3506.....	2005 Apr 18	1620	1720
F2M0841+3604.....	2005 Apr 24	1600	1716
F2M0915+2418.....	2005 Jun 5	1672	1776
F2M1012+2825.....	2005 Jun 13	2190	2250
F2M1113+1244.....	2005 May 26	1660	1760
F2M1118−0033.....	2005 Jul 14	1640	1752
F2M1151+5359.....	2005 Apr 20	1860	1972
F2M1507+3129.....	2005 Jul 28	2290	2340
F2M1532+2415.....	2005 Apr 24	1736	1840
F2M1656+3821.....	2005 Apr 19	1760	1876

We then performed photometry measurements on the images in the two bands. For this we used SExtractor (Bertin & Arnouts 1996) with parameters set as described in Benítez et al. (2004). We used the AB magnitude zero points from the ACS World Wide Web site. We extracted two magnitudes this way: first the isophotal corrected magnitude (assuming a symmetric Gaussian profile for the object) and then a 3″ aperture magnitude. A large difference between the two may indicate that a lot of the light comes from a galaxy component outside the nucleus. We also compared the magnitudes with the SDSS DR5 magnitudes. All quasars except F2M0729+3336 had SDSS imaging. Whenever the *HST* and SDSS magnitudes differ greatly, it means that the SDSS was not able to separate different components from the actual quasar due to its poor resolution. Table 4 presents the magnitudes.

The astrometry of ACS often has errors of up to 1.5″, so we shifted the WCS of the images using SDSS stars in the field as references. This greatly improved our astrometry, to within a radial rms error of 0.1″. We then compared these newly calibrated images with the FIRST data to confirm that the radio emission comes from the central nucleus or, in some cases, locate the likely position of the nucleus. The FIRST and SDSS surveys are fit to the same astrometric system and both have position errors less than 0.2″. In most cases the radio emission is associated with the brightest central optical component. For F2M1656+3821, the radio emission comes from the brightest of the three components. Yet for F2M0841+3604 the radio emission emanates from the center between the two brightest points. The lower σ contours are skewed a little toward the brightest source. It is not clear where the radio emission is coming from in this source.

4. ANALYSIS AND RESULTS

4.1. *Properties of the Quasars*

We performed quasar point-source subtraction and host galaxy fitting for the red quasars. We did perform the subtraction for the most irregular merging systems in our sample (F2M0841+3604, F2M1113+1244, F2M1532+2415, F2M1656+3821); however, these sources have multiple components or are extremely irregular, so the host galaxy fitting will likely be wrong. For the fitting and subtracting we used our own IDL program `fithost`.

F2M0729+3336

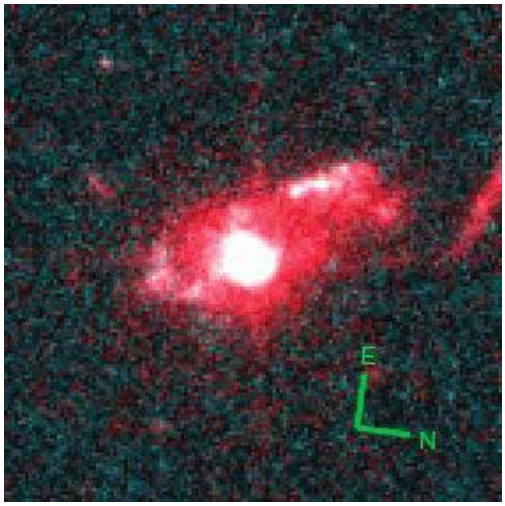

F2M0825+4716

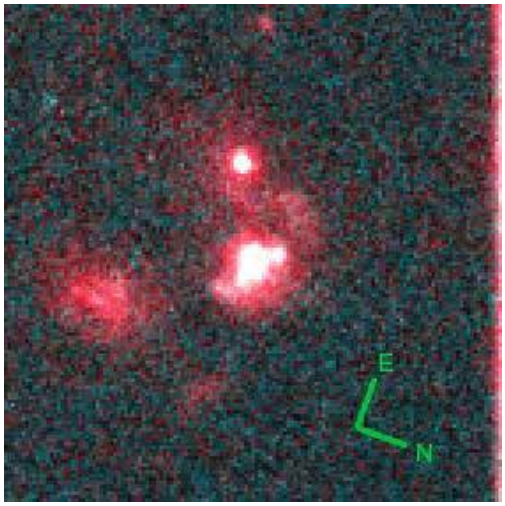

F2M0830+3759

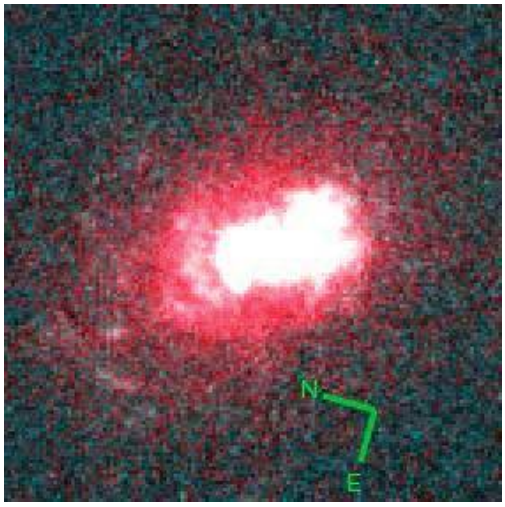

F2M0834+3506

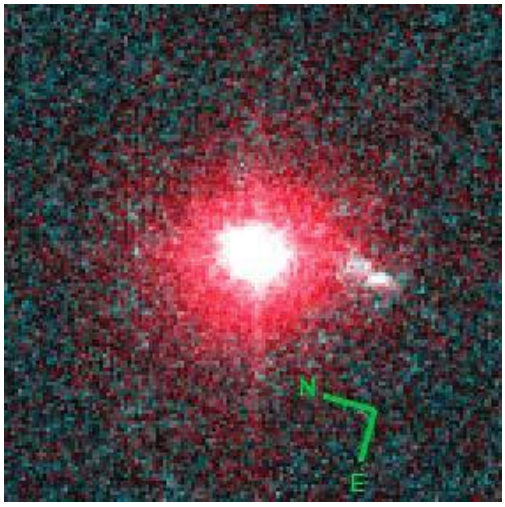

F2M0841+3604

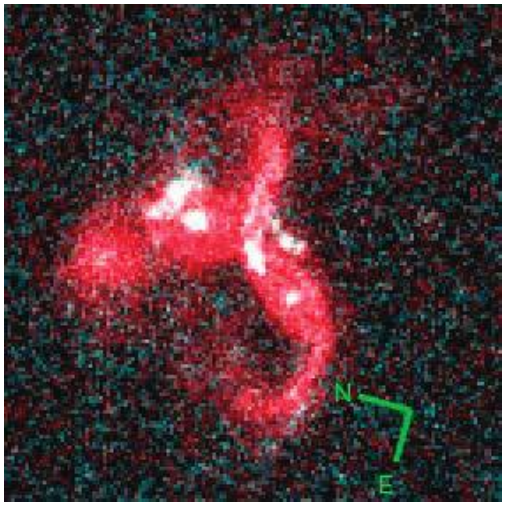

F2M0915+2418

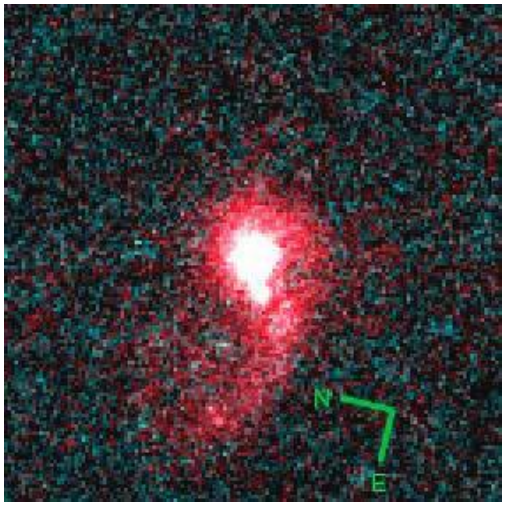

FIG. 2.—Color composites of the 13 red quasars. We use the *I*-band data for the red part and the *g* band for the blue and green parts of the composite. The images are $7'' \times 7''$. The g'-band cuts were set so that it the blue/green part of the image is somewhat more enhanced in comparison to the I_C-band data; the actual details from the host galaxies can be seen. The true color images would appear redder than shown here. For a quasar at redshift of $z \sim 0.7$, which is typical for our sample, $1''$ represents about 7 kpc.

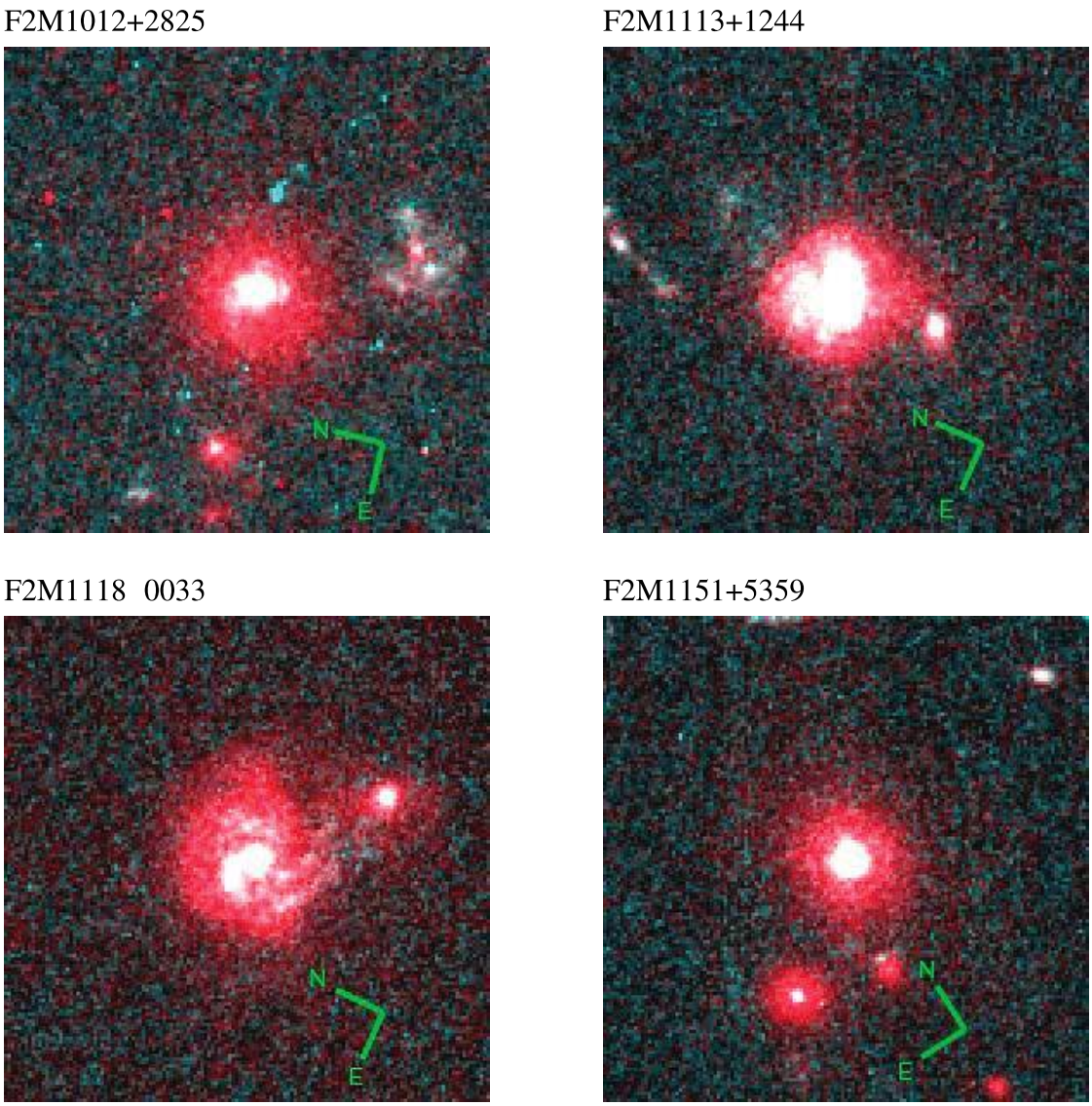

FIG. 2—*Continued*

It is based on the two-dimensional fitting technique of McLure et al. (2000) and has been successfully applied to ground-based AO data (Lacy et al. 2002). The program simultaneously fits and subtracts both point-spread function (PSF) and host galaxy; the host galaxy fitting is described in § 4.2.

PSF stars were observed at the end of the *HST* orbits, immediately after the quasars. Stars were chosen to be close to the quasars, so as to avoid extra overhead due to guide star acquisition, and to be bright enough to have a similar fluence to the quasar in short exposures. Observations were made with the stars as close as possible to the same position as the quasars on the detector, and with the same dither offsets, The only drawback to this technique was that the ACS 1K subarray had to be used for both the quasars and the guide stars to avoid excessive readout overhead. Since we were mostly interested in the quasars and their close companions this was not a major problem.

The `fithost` program was used in a mode where it automatically tries to fit the PSF-function to the brightest point in the image and then scale and remove it, so that the host galaxy can be subsequently fit. The center of the quasar and the host galaxy need not necessarily coincide. Starting parameters for the `fithost` program were derived using the IRAF program `imexam` and then refined with a second run. The first two postage stamp images in Figure 3 show the red quasars before and after PSF subtraction. For the sake of brevity we chose to only show the I_C-band results, since they have most contribution from the quasar and most incident flux. In the I_C band the flux from the PSF is typically similar to that of the host galaxies, but concentrated in the center of the image, which is why in Figure 3 we do not see glaring differences in the PSF-subtracted images from the original. In the g' band, the quasar is even fainter. The magnitude of the PSF/quasar after fitting is found in the first two columns of Table 5

The first result we can derive from the PSF fitting of the *HST* images is that the quasars are actually more obscured than deduced from the spectrum. In the *HST* g' band, which corresponds to rest-frame UV, we almost only see host galaxy contribution with the quasar being almost entirely extinguished. The $g' - I_C$ colors the fitted quasar PSFs are also redder than for the total system. While the mean SDSS g'—i' color for the total system is 1.92, the average $g' - I_C$ color for the quasar (just the PSF) is 0.61 mag redder at 2.53.

We then calculated the reddening for only the quasar by reddening the slope of the FBQS composite (accounting for emission lines that might have fallen within the passbands) to fit the

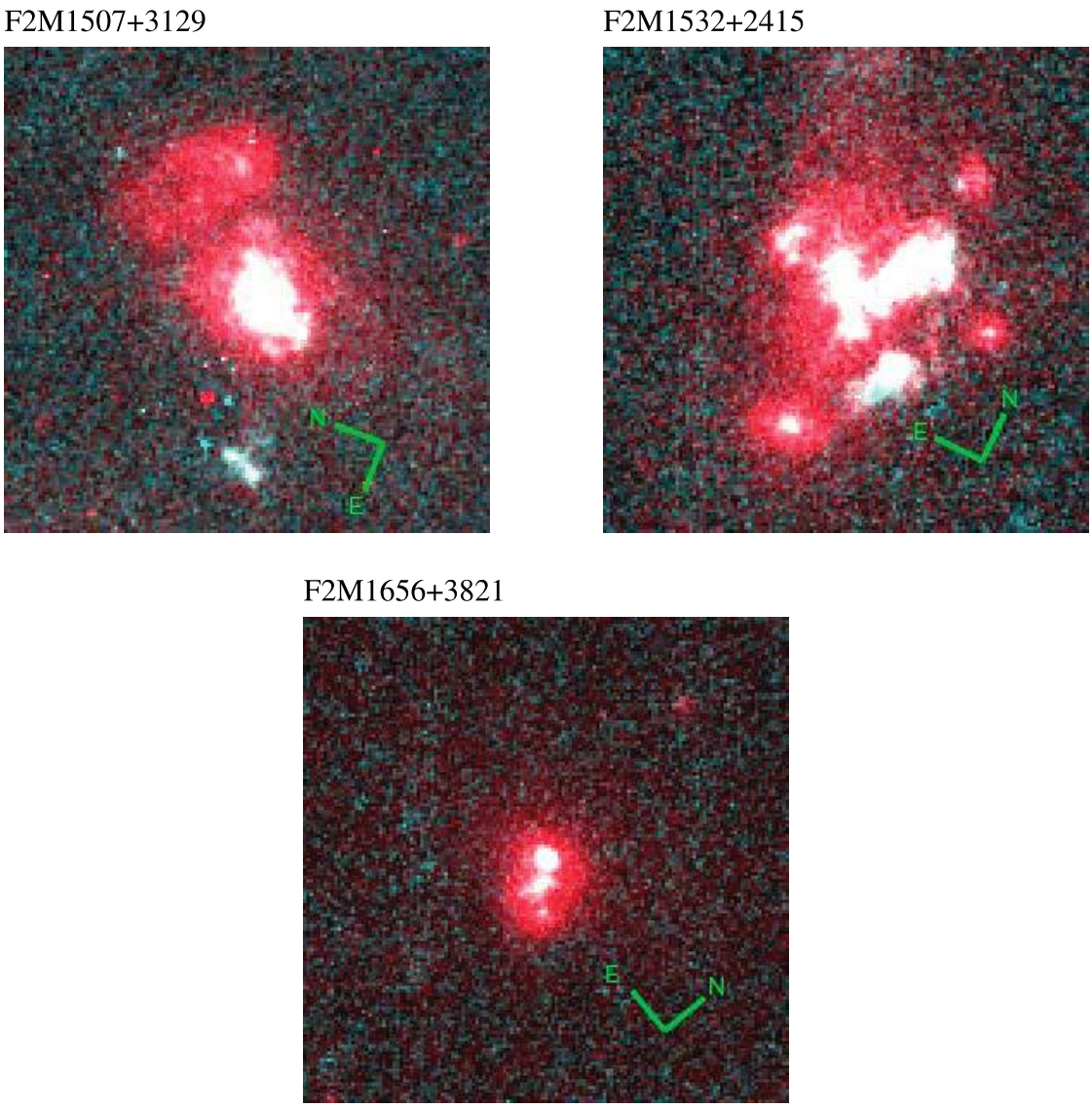

FIG. 2—*Continued*

$g' - I_c$ colors made by the PSF using the reddening curve described in § 2.1. Most of the objects which already had large $E(B - V)$ reddenings around 1.0 increase their reddenings and colors, while the objects where the reddening of the total system were close to 0.5 on average do not increase or decrease their reddening. Interestingly, the objects for which the fit of the reddened quasar composite broke down, mostly decrease their reddenings, implying that the host galaxy itself has enough starlight that is responsible for some of the red colors of our objects. There could also be scattering of the nuclear light into the host galaxy itself, but we assume that the deduced PSF magnitude is the total quasar magnitude, since we cannot assess the amount of scattering from the optical data alone.

Figure 4 shows the shifts of the objects colors and reddenings. The total magnitudes and reddenings are represented by the filled circles and the stars represent the quasar/PSF. Two of the quasars (F2M0841+3604 and F2M1656+3821) were not resolved in the SDSS, so the PSF magnitudes are much fainter than implied by

TABLE 3
SOURCES WITH MULTIPLE COMPONENTS

SOURCE	COMPONENT	SEPARATION		COMMENTS
		Arcseconds	Kiloparsec	
0841+3604	2	1.0	9.2	Wide separation
1012+2825	2	0.15	1.2	Resolved in g' band
1118−0033.....	2	0.40	2.8	One component, stellar
1532+2415	2	0.75	4.9	One component, stellar
1656+3821	3	0.80	5.89	Two components, stellar

TABLE 4
Comparison of Total Magnitudes

Source	Aperture (3″)		Isophot		SDSS (Petrosian)	
	mag_{I_C}	$mag_{g'}$	mag_{I_c}	$mag_{g'}$	mag_i	mag_g
F2M0729+3336	19.17 ± 0.05	21.71 ± 0.15	19.20 ± 0.05	21.82 ± 0.15	...	...
F2M0825+4716	21.04 ± 0.11	22.45 ± 0.21	21.05 ± 0.11	22.50 ± 0.21	18.93 ± 0.08	21.12 ± 0.17
F2M0830+3759	18.45 ± 0.03	20.24 ± 0.07	18.38 ± 0.03	20.19 ± 0.07	18.33 ± 0.03	20.06 ± 0.04
F2M0834+3506	18.57 ± 0.04	20.31 ± 0.08	18.57 ± 0.04	20.39 ± 0.08	19.07 ± 0.03	20.98 ± 0.08
F2M0841+3604[a]	20.45 ± 0.09	24.06 ± 0.44	20.23 ± 0.08	25.53 ± 0.51	20.10 ± 0.09	21.98 ± 0.23
F2M0915+2418	19.53 ± 0.06	20.68 ± 0.09	19.56 ± 0.06	20.77 ± 0.09	19.95 ± 0.06	20.63 ± 0.04
F2M1012+2825	20.23 ± 0.08	22.67 ± 0.23	20.24 ± 0.08	22.77 ± 0.24	20.38 ± 0.63	22.66 ± 0.64
F2M1113+1244	18.60 ± 0.04	21.02 ± 0.11	18.64 ± 0.04	21.03 ± 0.11	18.78 ± 0.03	20.78 ± 0.07
F2M1118−0033	19.46 ± 0.06	21.71 ± 0.15	19.31 ± 0.05	21.69 ± 0.15	19.41 ± 0.06	21.49 ± 0.13
F2M1151+5359	20.05 ± 0.07	21.41 ± 0.13	20.05 ± 0.07	21.50 ± 0.13	20.06 ± 0.11	21.31 ± 0.10
F2M1507+3129	19.48 ± 0.06	21.73 ± 0.15	19.39 ± 0.05	21.80 ± 0.15	19.73 ± 0.12	21.66 ± 0.13
F2M1532+2415[b]	19.46 ± 0.06	21.94 ± 0.16	19.20 ± 0.05	22.06 ± 0.17	19.09 ± 0.06	20.78 ± 0.10
F2M1656+3821	20.72 ± 0.10	23.65 ± 0.36	20.69 ± 0.10	23.68 ± 0.36	20.76 ± 0.20	23.54 ± 0.92

[a] *HST* magnitude quoted for brightest component. The different components are not resolved in SDSS.
[b] *HST* g'-band magnitute quoted for brightest component. The different components are not resolved in SDSS or *HST I* band.

SDSS. We mark these objects in Figure 4 in gray color; their shifts are likely to be wrong, but we include them in the figure for completeness.

From the $g' - I_C$ colors, magnitudes, and reddenings, we can then calculate the true luminosity for the quasar, since the absolute magnitudes calculated in § 2.1 from the spectrum had contamination from the host galaxy, especially in the bluer passband. Table 5 gives the new luminosities (corrected for reddening) determined from the quasar colors and magnitudes. The quasars are a bit more luminous on average, due to the fact that the quasar is more obscured than had been deduced from the spectrum. The quasars on average are still well above the quasar/Seyfert divide and much more luminous than the red quasar study conducted by Marble et al. (2003) so our claim that we are missing a large population of obscured AGNs is still valid.

4.2. *Properties of the Host Galaxies*

Before modeling the full host/quasar system, we obtained a constraint on the host galaxy magnitude. We did this by constraining the scaled PSF subtraction so that the residual was approximately flat in the center of the quasar host within a 3 pixel radius and declined monotonically outside that radius. We also obtained the lower limit of the host galaxy magnitude by subtracting the PSF until the central pixel was zero. The ''mono'' and ''zero'' magnitude are found in Table 6.

The host galaxies were modeled by fitting PSF plus galaxy model profiles (convolved by the PSF) by minimizing χ^2. Close to the center of the source, systematic errors from the PSF subtraction dominate, so to prevent those errors to dominate the fit, the inner 3 pixel radius was down-weighted by a factor of 0.5 to ensure that the χ^2 surface was fairly uniform across the fitting aperture. The position of the PSF and the galaxy nucleus was not held fixed; so in total we fit the flux, angle, axial ratio, and position of the host galaxy to the image. We tried to fit both elliptical and exponential profiles to the images; however, in all but one case (F2M1118−0033), the elliptical profile was best, so all our quoted values are for an elliptical profile.

Figure 3 shows the fitted elliptical galaxy and the residuals after PSF and model-galaxy subtraction in the third and fourth panels, respectively. Note that none of the galaxies are a perfect fit to an elliptical, however, there were some which came quite close, like F2M0915+2418. Also, two of the host galaxies, while they did not fit the elliptical profile well, did not show signs for interaction (F2M0834+3506 and F2M1151+5359). The fraction of 11 out of 13 systems showing interaction is much higher than the 2MASS red AGN fraction of one-third (Marble et al. 2003) and other unobscured quasar host galaxy studies. The fifth panel in Figure 3 shows the radial surface brightness profiles for the PSF subtracted images, and the solid line is the model applied with which they were fitted.

In the following paragraphs, when we discuss the host galaxies we mean the PSF-subtracted images and not the modeled host galaxies, to assess their magnitudes, morphologies, and comparison the quasar.

We measured the magnitudes of the host galaxies with SExtractor following the conventions above. The isophotal-magnitudes are quoted in Table 6. They were calculated in the same way the magnitudes were calculated in § 3. Note that in the cases where the total magnitude of the host galaxy is fainter than the limit denoted by the ''zero'' magnitude, the total host magnitude only refers to the central component of the galaxy, as the host galaxies often showed so large interactions that they are broken up and have various components.

The colors of the host galaxies are not particularly blue, so the host galaxies do not show large amounts of unobscured star formation. However, some of the extended components are blue, indicating the presence of either merger-induced star formation, or light associated with the quasar. This quasar light could be either scattered continuum, or extended line emission. The lack of a clear ionization cone morphology (with the possible exception of F2M0830+3759), however, would suggest that most of this blue light is from young stars.

We also measured the nucleus to host (N/H) ratios from these magnitudes (Table 6 for the I_C-band N/H). As discussed in § 4.1, the N/H for the g' band will be lower, because the quasar is more extinguished and most of the light in that band will come from the host. Overall, the luminosity of the hosts are on average, a little larger than those of the nuclei, such as the sample of IR-excess quasar sample of Surace et al. (2001). The relatively low N/H are in sharp contrast to the high N/H ratios of the luminous quasar sample of McLure et al. (1999), which is tied to the Dunlop et al. (2003) sample. However, the N/H ratios of our quasars are generally higher than the red quasar sample of Marble et al. (2003).

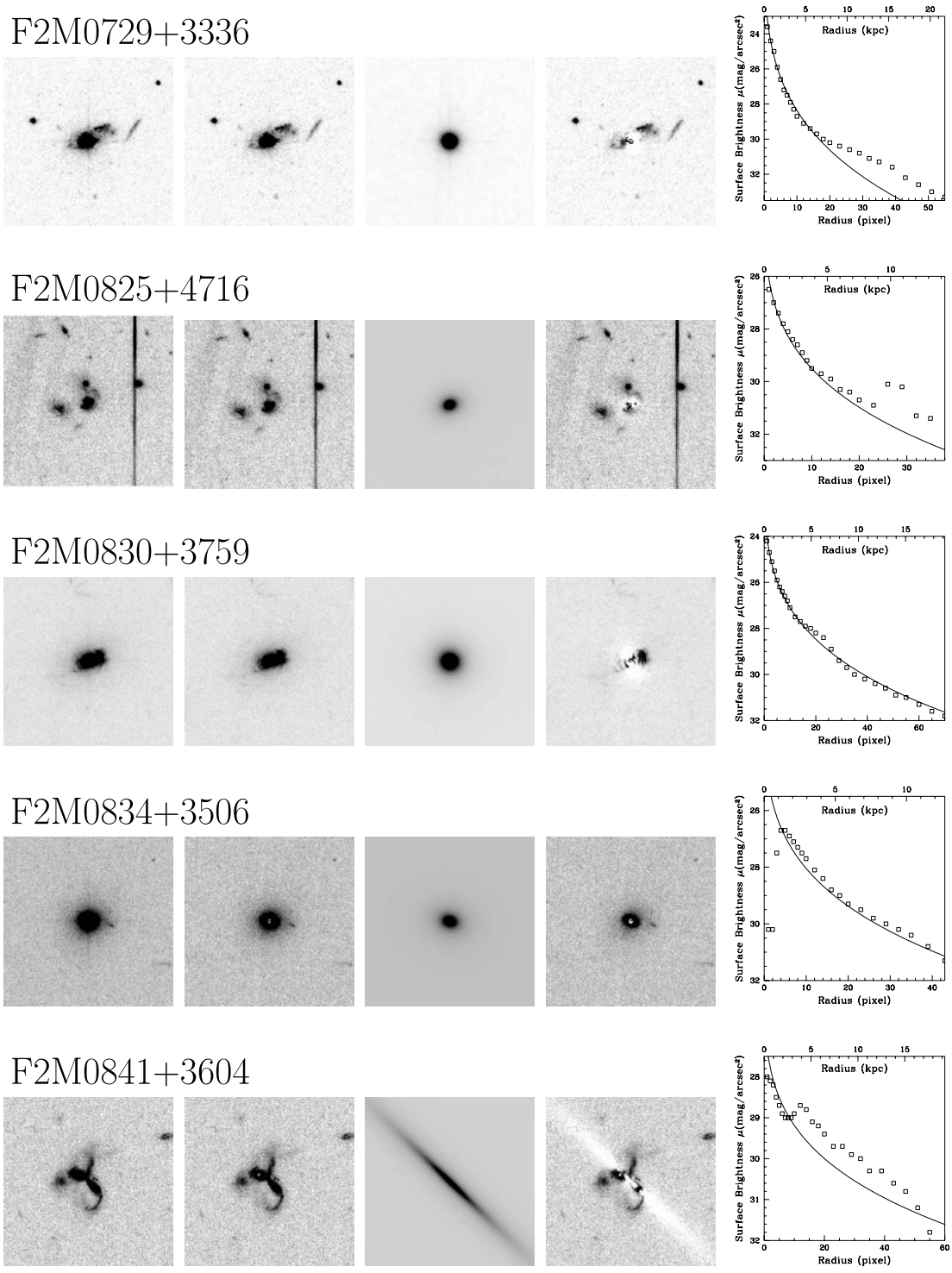

FIG. 3.—I_C-band results of PSF and host galaxy fitting. The first column shows an original postage stamp of the red quasar image, the second column the PSF-subtracted image, the third the best-fit elliptical model, the fourth the residual after subtracting the model and the fifth the radial surface brightness profile with the solid lines representing the elliptical fit.

We then calculated the absolute magnitudes (M_B) of the hosts adopting a 1 Gyr post starburst model from Bruzual & Charlot (2003) for the K-correction. At the typical redshifts of our sample ($z \sim 0.7$) $M_B^* = -20.30$ (Ilbert et al. 2006), so the host galaxies are around or a bit above L^* luminosity.

One measure of the extent of the host galaxy is the Petrosian radius r_P (Petrosian 1976). Very irregular or interacting systems tend to have high Petrosian radii, while compact ellipticals have a low r_P. The Petrosian radius is defined when the ratio of he surface brightness at the Petrosian radius and the average surface brightness at radii below reach a certain value η:

$$\eta = \frac{\mu(r_P)}{\bar{\mu}(r < r_P)}. \quad (2)$$

Following SDSS conventions, we set $\eta = 0.2$. Table 6 quotes the Petrosian radii of our systems. With one exception (the very compact F2M0729+3336), most have Petrosian radii around

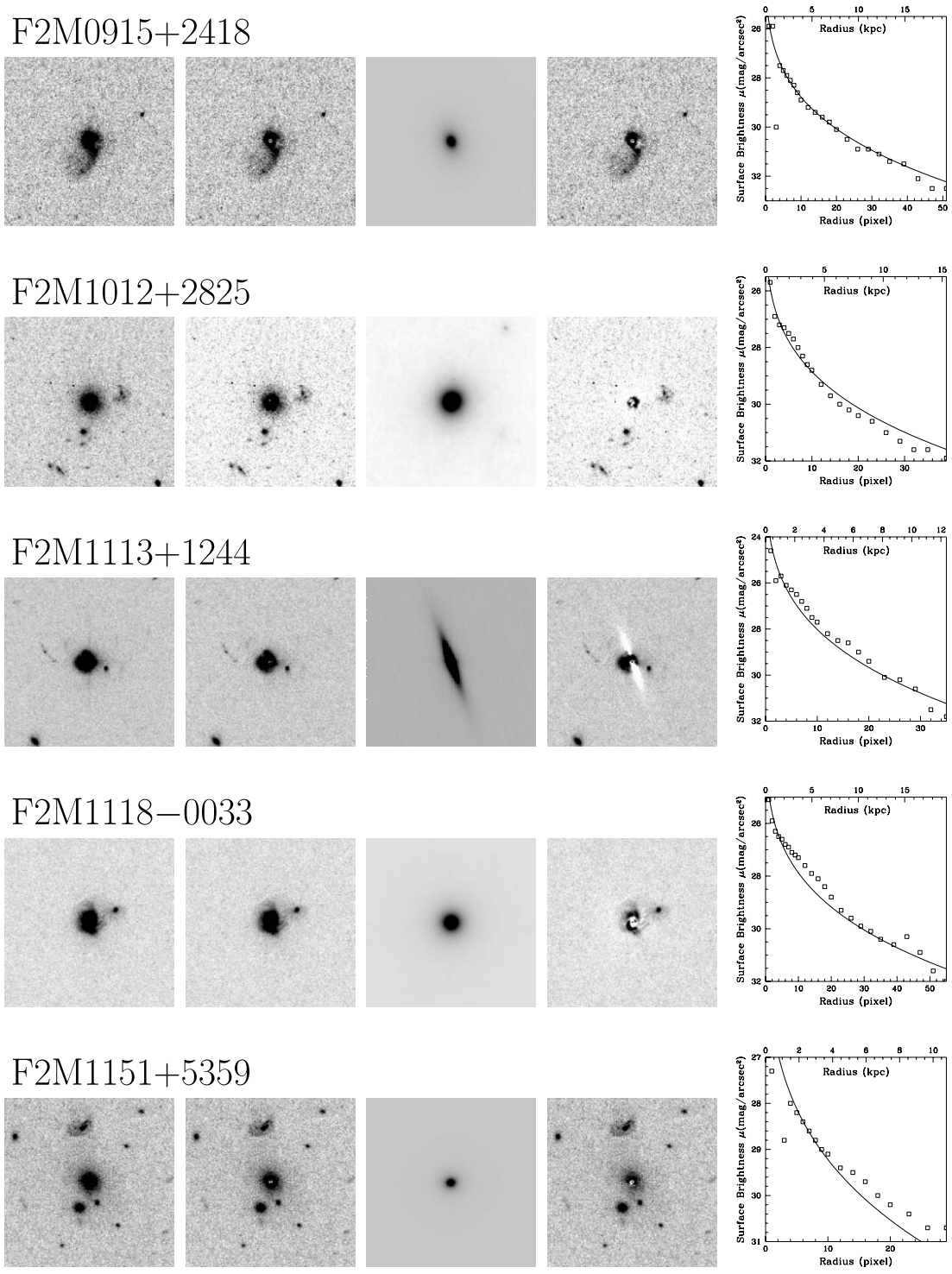

FIG. 3—*Continued*

1″–2.5″, which are normal for galaxies at those redshifts. When comparing those numbers to the surface density plots in Figure 3, one can notice that the nucleus ($r < r_P$) of the host galaxy often has an elliptical profile; only the most irregular systems such as F2M0841+3604 are irregular at low radii. Mostly, the interaction features only appear well beyond the Petrosian radius and usually have low surface brightness.

This could be an indication why many authors conclude that the host galaxies of luminous quasars are fit best mostly by elliptical profiles (e.g., Floyd et al. 2004), but find so few merger remnants. Perhaps with the overpowering AGN (high N/H ratios), the low surface brightness features, or interaction morphology signatures are lost. Recently, very deep imaging of some of the quasars studied by Dunlop et al. (2003) show either low surface brightness tidal tails or other merger remnants in the form of shells (Bennert et al. 2007) further supporting this point. The red quasars in this study are quite extinguished, so the host galaxy features are easier to discern. We tested how the tidal features can disappear in the presence of a bright quasar by adding point sources of different brightness (1, 3, and 10 N/H ratios) to the host galaxy image.

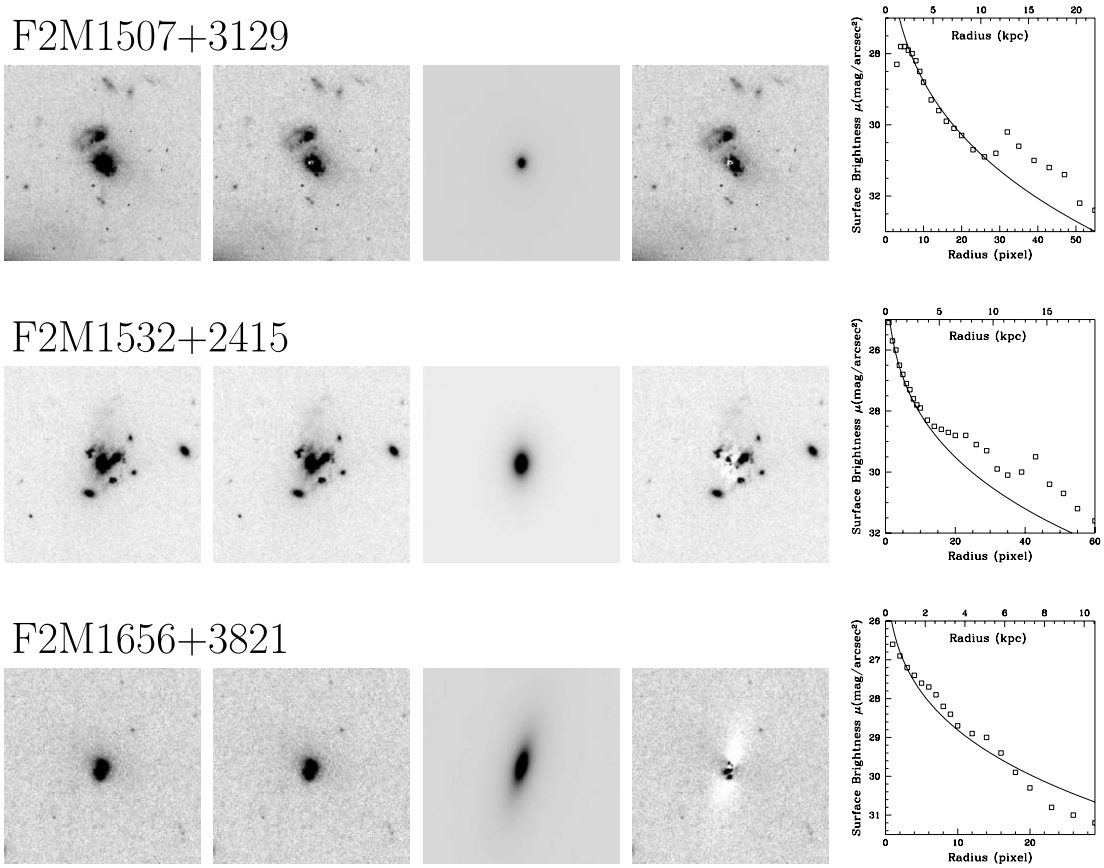

FIG. 3—*Continued*

When a PSF with a N/H ratio of 10 is added, the quasar is so bright that in all cases with exception of F2M0841+3604 the red quasars lose most of their interaction features and the quasar dominates the image (Fig. 5). Even so, after performing PSF subtraction on a N/H = 10 quasar+host system, the interactions should reappear. Also the red quasar host galaxies are in an earlier stage of the merger as we will see next.

As we already commented in § 3 the fraction of our red quasars showing interaction in their host galaxies is very high. Furthermore, all of the *dust*-reddened quasars, that is the quasars where the dust-reddening template fit best, show interaction. $E(B-V)$ seems to correlate weakly with the amount of interaction; the more obscured the quasar is, the more disturbed the morphology of the host galaxy is. We can arrive at these conclusions more or

TABLE 5
QUASAR (PSF) PROPERTIES

	PSF MAGNITUDES		$g-I$ COLORS		$E(B-V)$		LUMINOSITIES (M_B)	
SOURCE	mag_{I_C}	$mag_{g'}$	Total[a]	PSF[b]	Total[c]	PSF[b]	Total[c]	PSF[b]
F2M0729+3336	20.15 ± 0.07	25.20 ± 0.73	2.62[d]	5.05	0.83 ± 0.22	1.18 ± 0.16	−24.96	−26.83
F2M0825+4716	22.33 ± 0.21	23.65 ± 0.36	2.19	1.32	0.50 ± 0.35	0.40 ± 0.14	−21.94	−21.92
F2M0830+3759	19.51 ± 0.06	22.62 ± 0.22	1.73	3.11	0.80 ± 0.15	1.29 ± 0.12	−22.73	−23.07
F2M0834+3506	18.95 ± 0.04	21.17 ± 0.11	1.91	2.22	0.53 ± 0.10	0.87 ± 0.06	−22.90	−23.80
F2M0841+3604	21.88 ± 0.17	25.11 ± 0.70	1.88	3.23	1.05 ± 0.64	1.10 ± 0.27	−21.03	−21.61[e]
F2M0915+2418	19.88 ± 0.07	20.99 ± 0.10	0.68	1.11	0.53 ± 0.36	0.31 ± 0.04	−23.69	−24.43
F2M1012+2825	21.17 ± 0.12	23.50 ± 0.33	2.28	2.33	0.66 ± 0.12	0.60 ± 0.12	−24.37	−24.26[e]
F2M1113+1244	19.11 ± 0.05	22.87 ± 0.25	2.00	3.76	1.01 ± 0.24	1.17 ± 0.09	−25.08	−25.45
F2M1118−0033	22.00 ± 0.18	23.33 ± 0.32	2.08	1.33	0.72 ± 0.26	0.48 ± 0.15	−22.97	−21.76
F2M1151+5359	20.48 ± 0.09	22.12 ± 0.18	1.25	1.59	0.47 ± 0.13	0.47 ± 0.07	−23.31	−23.78
F2M1507+3129	19.78 ± 0.07	22.67 ± 0.23	1.93	2.89	0.54 ± 0.13	0.69 ± 0.08	−24.27	−26.24
F2M1532+2415	21.14 ± 0.12	24.42 ± 0.51	1.69	3.28	0.90 ± 0.53	1.12 ± 0.21	−20.46	−22.45[e]
F2M1656+3821	23.46 ± 0.35	25.11 ± 0.70	2.78	1.65	0.55 ± 0.57	0.54 ± 0.28	−20.86	−20.66[e]

[a] SDSS.
[b] *HST*
[c] Spectrum.
[d] No SDSS photometry, we use *HST* values.
[e] Luminosity is only for one nucleus.

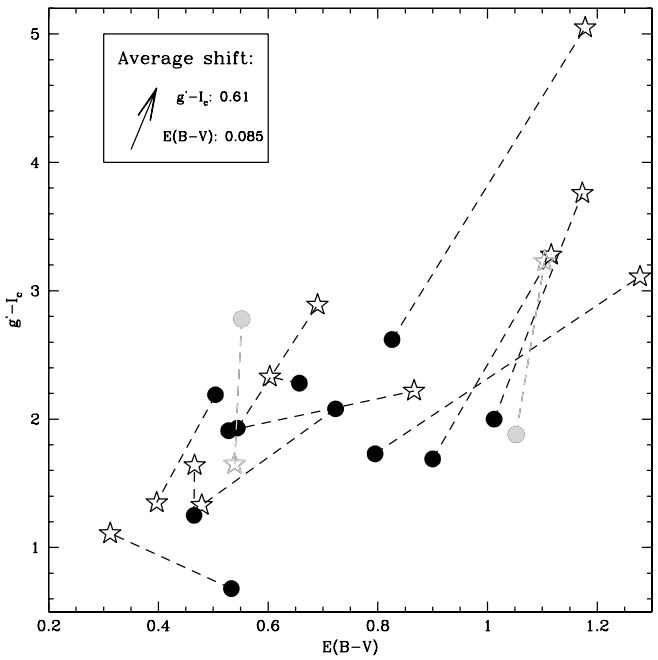

FIG. 4.—Plot of $g' - I_C$ color vs. $E(B - V)$ reddening. The filled dots represent the magnitudes and reddenings for the total system. The magnitudes are from SDSS data and do not differ much from *HST* photometry and the $E(B - V)$ reddening is from spectral fitting. The open stars represent quasar (PSF) color and reddenings derived from *HST* PSF photometry. We included lines to show how the values shifted. On average the quasar has a 0.61 mag redder color and higher $E(B - V)$ of 0.085 mag. [*See the electronic edition of the Journal for a color version of this figure.*]

less "by eye," but we support our claims by parameterizing the host galaxy morphology with their Gini coefficients and their concentration indices.

The Gini coefficient is a nonparametric approach to classifying a galaxy and can therefore be easily applied to irregular galaxies or highly merging systems. It is a measure of the cumulative distribution of a galaxy's pixel values and is a good alternative approach to quantifying the amount of interactions in galaxies. The Gini coefficient is correlated with the concentration index of galaxies for spiral and elliptical galaxies (Abraham et al. 2003) and anticorrelated with the concentration index for ULIRGs and other highly irregular systems (Lotz et al. 2004). A high Gini coefficient therefore indicates either a high level of interactions or a highly concentrated elliptical galaxy, while a low Gini coefficient indicates either spiral galaxies or low surface brightness galaxies.

We calculated the Gini coefficient of the host galaxies of the red quasars by following the conventions in Abraham et al. (2003). Based on the formalism by Glasser et al. (1962), if we sort the pixels X_i's flux into increasing order, the Gini coefficient can be calculated by

$$G = \frac{1}{\bar{X} n(n-1)} \sum_{i}^{n} (2i - n - 1) X_i. \quad (3)$$

However, we took notice of the warning by Lotz et al. (2004) and tried to create segmentation maps at the $\mu(r_P)$, the flux threshold above which pixels are assigned to the galaxy. For that we cut out galaxy postage stamps cutouts by eye and included only pixels within that cutout that had a surface brightness higher than $\mu(r_P)$. The Gini coefficient was then computed of the distribution of *absolute* flux values of the pixels, which corrects for the areas in the center which were PSF-oversubtracted. The Gini coefficients G can be found in Table 6.

The concentration index measures the ratio of the flux within an inner radius to that within and outer circular or elliptical aperture. The main difference in the definitions by different authors is the choice of the radii or semimajor axes of the two apertures. Conselice et al. (2003) adopts a ratio between the radii containing certain percentages of the total light. Abraham et al. (1994) uses a flux ratio between two normalized radii α and 1, where $E(1)$ is the area encompassing 2 σ flux and α is typically set to 0.3:

$$C = \frac{\sum \sum_{i,j \in E(\alpha)} I_{ij}}{\sum \sum_{i,j \in E(1)} I_{ij}}. \quad (4)$$

Since Abraham et al. (2003) has already linked the Gini coefficient to the concentration index via a unity slope, we decided to use the concentration index defined in equation (4) instead of the Conselice et al. (2003) definition. We chose the total flux as the flux within $1.5r_P$ and $E(\alpha)$ as the flux within $0.45r_P$. From that ratio we are able to obtain C, which is quoted in Table 6.

Figure 6 shows the Gini coefficient plotted against the $E(B - V)$ reddening derived from the HST quasar magnitudes on the left side and the concentration index over the same $E(B - V)$ on

TABLE 6
HOST GALAXY PROPERTIES

	Host mag$_{I_C}$			Host mag$_{g'}$			Luminosities			Morphologies		
Source	Zero	Mono	Total	Zero	Mono	Total	N/H[a]	M_B	L^*	r_P (pix)	G	C
F2M0729+3336.....	20.71	19.97	19.78 ± 0.06	21.80	21.80	21.78 ± 0.15	0.711	−22.32	6.4	03.8	0.69	0.36
F2M0825+4716.....	20.07	19.99	21.48 ± 0.14	21.71	21.58	22.95 ± 0.26	0.470	−20.02	0.8	29.3	0.54	0.42
F2M0830+3759.....	18.96	18.75	18.86 ± 0.04	20.53	20.22	20.31 ± 0.08	0.550	−21.02	1.9	25.9	0.57	0.41
F2M0834+3506.....	19.96	19.87	19.77 ± 0.06	22.66	22.56	21.13 ± 0.11	2.089	−20.42	1.1	37.5	0.52	0.55
F2M0841+3604.....	19.96	19.90	20.40 ± 0.09	21.57	21.54	23.04 ± 0.27	0.256	−20.22	0.9	53.7	0.52	0.30
F2M0915+2418.....	20.72	20.64	20.82 ± 0.10	25.58	23.83	22.91 ± 0.25	2.355	−20.90	1.7	24.0	0.49	0.38
F2M1012+2825.....	20.56	20.44	20.87 ± 0.11	22.12	21.99	23.49 ± 0.33	0.759	−21.15	2.2	19.8	0.59	0.52
F2M1113+1244.....	20.06	19.76	19.75 ± 0.06	21.12	21.87	21.31 ± 0.12	1.803	−21.28	2.5	18.6	0.68	0.55
F2M1118−0033.....	19.34	19.24	19.51 ± 0.06	20.95	20.91	22.70 ± 0.22	0.101	−21.53	3.1	22.6	0.59	0.42
F2M1151+5359.....	20.03	19.99	20.99 ± 0.11	22.70	22.46	22.43 ± 0.20	1.528	−20.41	1.1	49.6	0.39	0.41
F2M1507+3129.....	20.10	20.07	20.96 ± 0.11	22.24	22.09	22.45 ± 0.21	2.858	−21.18	2.2	48.5	0.57	0.49
F2M1532+2415.....	19.15	19.05	19.39 ± 0.05	20.77	20.69	22.20 ± 0.18	0.194	−21.27	2.4	33.4	0.60	0.40
F2M1656+3821.....	20.58	20.45	20.77 ± 0.10	22.22	22.14	24.96 ± 0.62	0.039	−20.47	1.1	20.3	0.59	0.44

[a] Nucleus-to-host ratios from I_C-band magnitudes. Zero and monoton are model magnitudes; therefore they do not have errors.

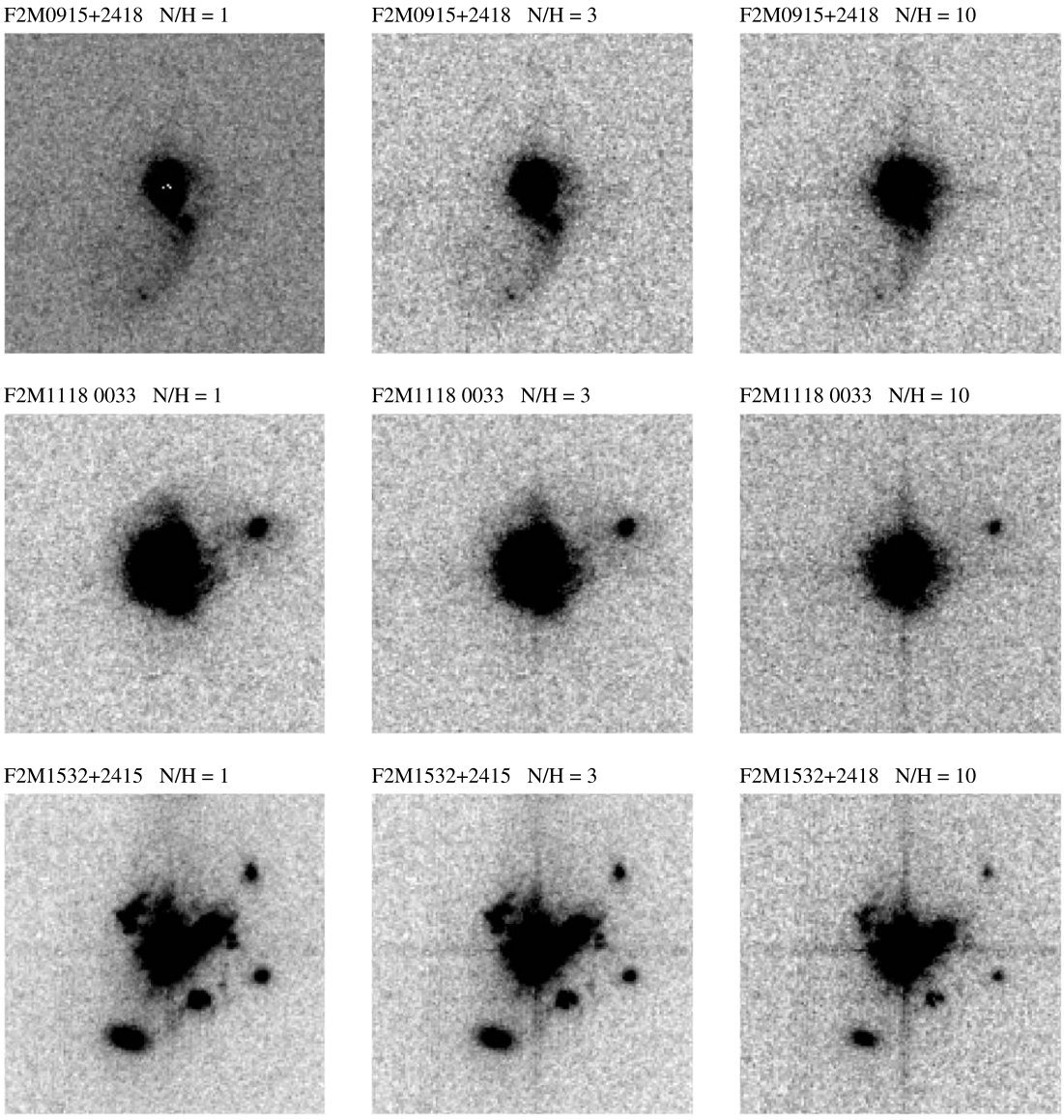

FIG. 5.—Host galaxies with artificial PSF added. The images show different nucleus to host ratios in increasing order. When the nucleus has the same magnitude as the host galaxy, which is the case for the red quasars in this sample, the interactions are clearly visible, such as the tidal connection in F2M1118−0033 or the strong halo in F2M1532+2415. With a nucleus to host ratio of 10, most of the features have disappeared and the PSF clearly dominates, as is typical in unobscured quasar sampled.

the right side. While there is a weak correlation between the Gini coefficient and the reddening, we find no correlation between the concentration index and $E(B-V)$. As mentioned before, high Gini coefficient and low concentration indices are an indication for interaction or merger, since the brightest flux pixels are highly concentrated in a few pixels (high G), but those pixels are not in the center (low C). This seems to be the case in the systems with the highest $E(B-V)$ in our sample, while the hosts of quasars with lower $E(B-V)$ tend to have both Gini coefficients and concentration indices more consistent with those of normal, undisturbed galaxies Abraham et al. (2003). On the lower panel of Figure 6 the concentration index is plotted against the Gini coefficient, with the unity slope shown. Only the two undisturbed galaxies (F2M0834+3506 and F2M1151+5359) are above this slope, with the rest having high Gini coefficients in relation to their concentration indices, again implying high-interaction features.

While we could already see those results "by eye," these galaxy parameters are affirmation to the result that the higher the reddening in the quasar, the higher the chance of interaction in the quasar host. Furthermore, if the reddening in the spectrum fits a dust-reddening template well, it is also a good indicator for evidence of interaction. Nonetheless, these results are based only on 13 highly heterogeneous systems, so further observations are needed to improve number statistics and to confirm this claim.

5. NOTES ON INDIVIDUAL QUASARS

While most of the quasar host galaxies show some degree of irregularity and evidence for merger, it is worth it to look at the quasars on an individual basis to further inspect some peculiarities in some of the objects.

5.1. *F2M0729+3336*

This is the only quasar for which SDSS information was not available. Even though we detected only 6 photons in the X-ray observations, all of them are in the hard band, giving this source a hardness ratio of 1.0 and therefore implying a high column density.

The spectrum has strong Ca H+K absorption lines, but the spectral reddening does fit a dust extinction law quite well longward

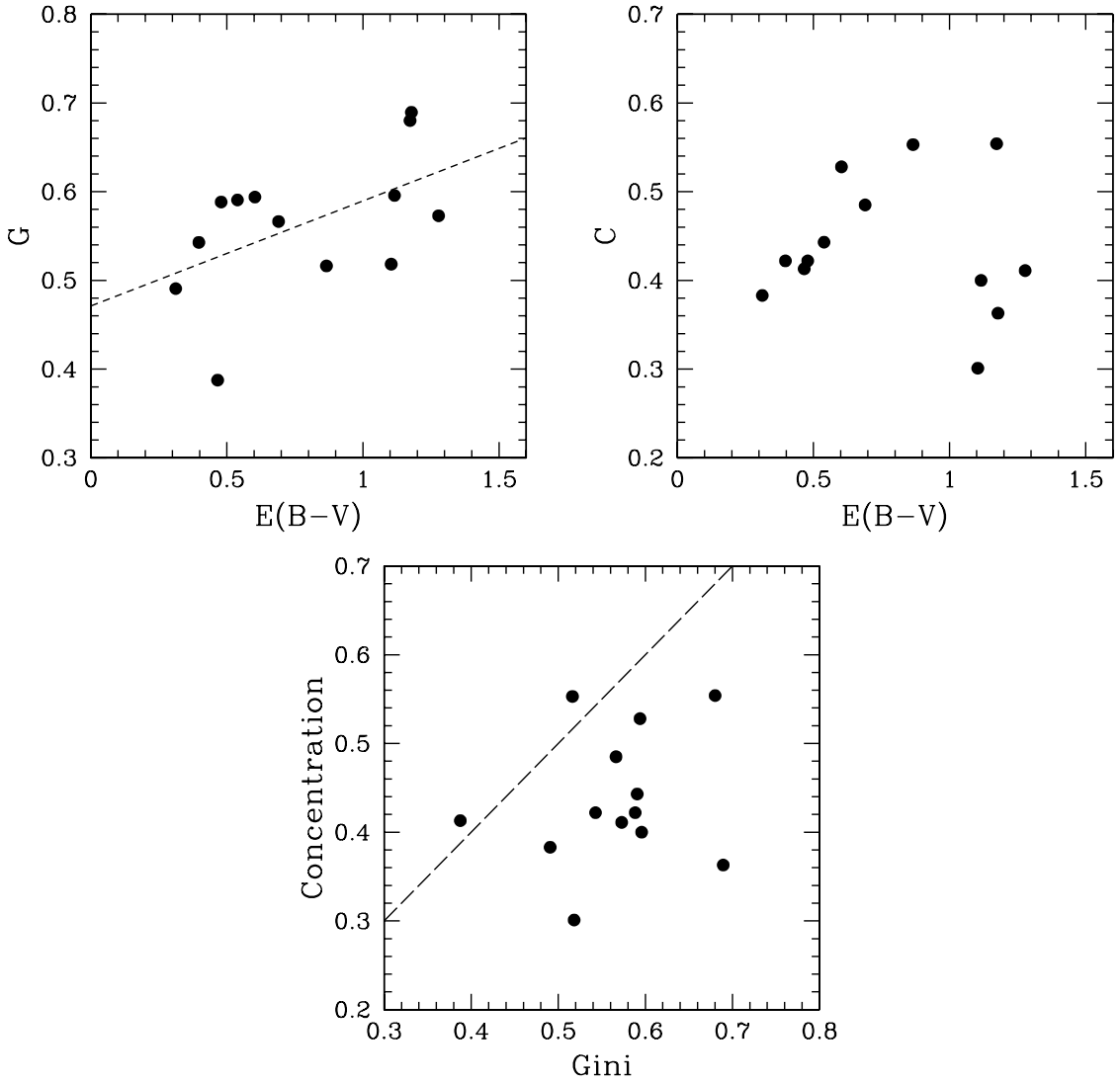

FIG. 6.—*Top left:* Gini coefficient vs. reddening. There is a weak correlation between the Gini coefficient and the reddening (*dashed line*). High Gini coefficients indicate either highly irregular systems, such as ULIRGs, or very compact ellipticals. *Top right*: Concentration index vs. reddening. For single systems the Gini coefficient and the concentration index are correlated. The fact that for high reddening we do not necessarily have high concentration indices means that the systems are highly disturbed, usually with more than one nucleus. *Bottom*: Concentration index vs. Gini coefficient. No correlation is found in our sample in contrast to other studies of single galaxies, indicating that a many of the red quasar hosts are in a merger status. The dotted line is the unity correlation found by Abraham et al. (2003). All but two host galaxies (the two undisturbed ones) of the F2M red quasars have higher Gini coefficients than implied from their concentration indices.

of about 5000 Å, so the host galaxy contribution to the red optical light in the spectrum is not going to make a large impact.

This particular system has a very compact elliptical host, with a very small Petrosian radius and large Gini coefficient. Beyond that however, large tidal tails extend out to over 20 kpc on both sides of the host, which is evidence for a recent merger event. This makes the total size of the host galaxy over 35 kpc. In the g' band, the quasar (PSF) contribution is almost nondetectable, making this the system with the largest shift in $g' - I_C$ color of the PSF relative to the total emission from the host.

5.2. *F2M0825+4716*

This looks like a type 2 quasar in the optical spectrum. The color of the quasar (PSF) would suggest that also. However, the Spex IR spectrum shows broad quasar lines, however, and a much redder spectral slope than implied by the optical continuum, which is probably dominated by host galaxy emission. The image shows that while the central component is fit well by an elliptical galaxy, there is a tidal bridge linking the central galaxy to a companion nearby.

The optical spectrum shows double-peaked narrow emission lines, separated by about 600 km s^{-1}. The higher redshift set has relatively strong Balmer lines and [O II]3727 emission at $z = 0.803$, and probably corresponds to the systemic redshift of the host galaxy. The blueshifted component at $z = 0.800$ is of higher ionization and probably corresponds to a high-ionization outflow.

5.3. *F2M0830+3759*

This quasar has the lowest redshift in our sample, therefore features close to the nucleus will be more easily observable. The *HST* image in fact shows a lot of irregularity near the nucleus with shells of material along the major axis, either side of the nucleus. They almost cancel each other out in the radial profile plot, resulting in a deceptively smooth radial profile, while in reality the host galaxy is very disturbed.

F2M0830+3759 was also observed with *Chandra* and has a very high X-ray flux (Urrutia et al. 2005). The X-ray spectrum shows a very broad iron Kα line, hinting that we are looking into the broad-line region of the quasar. It has a moderate absorption, but a higher than usual spectral slope ($\Gamma \approx 2.9$). This is also the only

object for which we have a gas:dust ratio, which is about 5 times Galactic value. While dusty, it is well within the 3–100 times Galactic value range deduced by Maiolino et al. (2001).

5.4. *F2M0834+3506*

The red quasar system has almost no evidence for interaction. The profile could fit an addition of elliptical profiles, but the morphology could also represent merger remnant shells. However, there are no extended features or tidal tails.

It is unclear whether the blue component just to the north of the quasar is associated with it, or whether it is an unrelated object close to the line of sight. There are broad Hα and Hβ emission lines $\sim$5000 km s^{-1} blueward of the quasar's redshift, which could be associated with that component and/or with the quasar.

5.5. *F2M0841+3604*

This object shows the most irregular morphology in the host galaxy of the *HST* images. While the optical image clearly shows two bright nuclei, of which either or both could be the quasar, the radio images (from FIRST and also 6 cm VLA A-array observations) show a steep spectrum point source right in between the two bright optical components. This raises the question of where the active nucleus actually is.

In addition to the *HST* and VLA images, F2M0841+3604 has been observed with *Chandra* (Urrutia et al. 2005). The *Chandra* photons are very hard. Unfortunately, the X-ray image had only 7 counts, so the position error on where the X-ray emission comes from is quite large. However, the *Chandra* photons appear to be spread out, so the X-ray emission could come from both nuclei. Overall, this is our most spectacular example of a young evolutionary merger state.

5.6. *F2M0915+2418*

F2M0915+2418 is the quasar which fits an elliptical profile best. However, a clear *tail* is seen extending to the east, indication a recent interaction.

5.7. *F2M1012+2825*

This red quasar displays two nuclei only 0.15″ (1.2 kpc) apart, which would have been missed in ground-based observations. The two nuclei are pointlike and especially easy to detect in the g' band, but the nucleus appears very "smeared" in the I_C-band image. The fitting of quasar and host galaxy is therefore impossible. The quoted luminosities for the quasar are only for one component, so the total nuclear luminosity is much higher than $M_B = -24.26$.

The rest of the host galaxy does not appear very disturbed and also here the central component fits an elliptical profile, were it not for that second nucleus. There is some blue emission north of the galaxy, but again, we do not know if it is associated with the quasar host.

5.8. *F2M1113+1244*

While the position of the quasar is quite certain, because of the clear stellar-like feature, it is noteworthy that the rest of the host galaxy consists of several bright knots, with a low surface brightness tidal tail extending to 30–35 kpc from the galaxy.

5.9. *F2M1118−0033*

The image for this red quasar shows it to be a clear merger with a nucleus and two compact components, one near the nucleus and the other one at the end of the two tidal tails trailing the system. This is the only system for which an exponential profile fit the host galaxy better than an elliptical (but only near the nucleus).

The optical spectrum for F2M1118−0033 shows a 4000 Å Balmer break, and a red spectral slope which appears to be dominated by the host galaxy. The infrared spectrum Glikman et al. (2004) also fails to show obvious broad emission lines, but does show a significant rise in K band, probably from quasar light.

5.10. *F2M1151+5359*

F2M1151+5359 is the quasar also fits an elliptical profile quite well, but there is still some residual in the host galaxy after model subtraction in the I_C band. The blue band fits almost perfectly. So this would be comparable to other "normal," bright, blue quasars, which have an undisturbed elliptical galaxy as a host. The spectrum shows asymmetric profiles in the emission lines and narrow Mg II absorption lines very close to the quasar redshift.

5.11. *F2M1507+3129*

This is the highest redshift red quasar imaged with ACS. The spectrum fits dust reddening quite well. Also here the central component can be well fit by an elliptical galaxy, but there is a low surface brightness tidal bridge connecting it to the red companion nearby. F2M1507+3129 is thus a very large (35 kpc) and spectacular merger at $z \sim 1$.

5.12. *F2M1532+2415*

HST imaging of F2M1532+2415 displays a truly disturbed host, with many components and no clear evidence of where the quasar is located among the constituents of the host galaxy. Radio maps show the synchrotron radiation coming from the central red component. They also show that this quasar is actually a classical Fanaroff-Riley type II radio double (FR II; Fanaroff & Riley 1974), with the outer components being over 1′ away from the central source.

The optical spectrum shows a very narrow Hβ line and no broad Mg II line, but in the infrared Paβ is broad. The quasar host shows extreme interaction.

5.13. *F2M1656+3821*

This optically faint object shows almost only host galaxy emission in the optical part of the spectrum, but in the near-infrared there is a very red continuum and a broad Paβ line. There are three components in the *HST* image, two pointlike and one elliptical. The radio flux points to the emission coming from the brightest (southwest) optical point source. The morphology of F2M1656+3821 could suggest that the system is a gravitational lens with the lensing galaxy lying between the two point sources. The reddening for this system might stem from the lensing galaxy and not the quasar itself, as is implied by the host galaxy's very red colors. However, the lack of any arclike morphology in the outer optical components and the lack of spectral features at lower redshift in this object's spectrum argues against the lensing hypothesis.

6. CONCLUSIONS

We have observed and analyzed a sample of 13 highly reddened, luminous quasars from the F2M survey Glikman et al. (2007) with ACS in both I_C and g' band to study their host galaxies. The images show interactions in 85% of the objects and clear evidence for mergers such as tidal tails and multiple nuclei. We fitted model PSF and galaxy profiles to the images. Within the nuclear region, most galaxies fit an elliptical profile, in accordance with quasar

host studies such as Dunlop et al. (2003), but outside of the nuclear region this fit is no longer valid as merger features become clear.

After performing PSF-fitting, the quasar displays even redder colors and reddenings than implied from SDSS imaging and ESI spectra, showing that the optical magnitudes of the quasars are significantly contaminated by the host galaxies in low-resolution data. Five of our galaxies show very dramatic, likely multiple merger morphologies, reminiscent of the simulations of high-z quasar hosts by Li et al. (2007). There is a wide range in merger phase, with some of our quasar hosts in an apparently early part of the merger sequence where the merging galaxies still retain their identity (F2M0841+3604), through to later stages with multiple nuclei (F2M1113+1244; F2M1012+2825), and objects at the final merger stage with only a single nucleus and a tidal tail remaining (F2M0915+2418). This would be consistent with quasar activity being triggered relatively early in an interaction, and continuing through the merger process.

We calculated the Gini coefficients and the concentration indices of the host galaxies and found a correlation of the Gini coefficient with reddening. The systems with the highest quasar $E(B-V)$ did not have high concentration indices consistent with their high Gini coefficients, which implies that the host galaxies have bright, compact components outside of the nuclear region. Using this as a measure of interaction, it seems that the amount of interaction is weakly correlated with how obscured the quasar is.

Floyd et al. (2004) studied a sample of 17 normal quasar hosts with *HST* which are closest to our sample in terms of luminosity and redshift. Their sample spanned $-24 < M_V < -28$ in quasar luminosity and $0.3 < z < 0.42$ in redshift. Consistent with previous studies, only a small fraction of interactions/mergers were seen (they have only one object out of 17 with definite signatures of an interaction). However, sensitive observations of the hosts of unreddened quasars of similar luminosity are difficult, so it is possible that some signs of interaction such as faint tidal tails and multiple nuclei close to the quasar will have been missed. Our correlation of reddening with morphology argues against this, but our observed correlation is only weak. However, Figure 5 also shows obvious signs of merger even at nucleus to host ratios of 10. Another possible source of bias is that, while none of the red quasars is radio-loud, these objects are all radio-selected, and fall into the ''radio intermediate'' category. The fact that all of our quasars are disturbed in comparison to, e.g., the Marble et al. (2003) sample, could be a selection effect. White et al. (2007) find that quasars with redder colors than the SDSS composite tend to have higher radio-fluxes.

These caveats aside, our results may explain why only about 30% of quasars with obvious signs of mergers and interactions have been found (Guyon et al. 2006; Marble et al. 2003). Reddening by dust from the host galaxy seems to be the most likely explanation for the redness of the F2M quasars. The host morphologies and colors are consistent with dusty, merging galaxies. If these objects were red because the line of sight just grazes the torus, we would expect less disturbed host morphologies, in line with those of normal quasars. Host galaxy reddening of the quasar, while only mild in our cases (and much less than nuclear reddening by an edge-on torus) can nevertheless be sufficient to remove the objects from optically selected quasar samples (or at best render them a small minority in such a sample). Given that these kind of dust-reddened type-1 quasars like these make up about 30% of the total in mid-IR selected samples, this means the fraction of quasar hosts associated with mergers has been significantly underestimated in the past. Our result is thus consistent with theories in which quasars start their lives obscured by dust, and only appear in optical or soft X-ray surveys after the dust along the line of sight to the nucleus has been cleared by quasar winds (Sanders et al. 1989; Sanders & Mirabel 1996; Springel et al. 2005; Hopkins et al. 2007a).

We thank Elinor Gates for assistance with writing the `fithost` program. We also thank Wim de Vries for help with the ACS astrometry.

This work was partly performed under the auspices of the US Department of Energy, National Nuclear Security Administration by the University of California, Lawrence Livermore National Laboratory, under contract DE-AC52-07NA27344. Funding for this project was supplied by Hubble grant 10412.

This publication makes use of data products from the Two Micron All-Sky Survey, which is a joint project of the University of Massachusetts and the Infrared Processing and Analysis Center/California Institute of Technology, funded by the National Aeronautics and Space Administration and the National Science Foundation.

This publication makes use of the Sloan Digital Sky Survey. Funding for the SDSS and SDSS-II has been provided by the Alfred P. Sloan Foundation, the Participating Institutions, the National Science Foundation, the US Department of Energy, the National Aeronautics and Space Administration, the Japanese Monbukagakusho, and the Max Planck Society, and the Higher Education Funding Council for England. The SDSS Web site is http://www.sdss.org/.

REFERENCES

Abraham, R. G., Valdes, F., Yee, H. K. C., & van den Bergh, S. 1994, ApJ, 432, 75
Abraham, R. G., van den Bergh, S., & Nair, P. 2003, ApJ, 588, 218
Antonucci, R. 1993, ARA&A, 31, 473
Becker, R. H., White, R. L., & Helfand, D. J. 1995, ApJ, 450, 559
Bennert, N., Canalizo, G., Jungwiert, B., Stockton, A., Schweizer, F., Lacy, M., & Peng, C. 2007, BAAS, 209, 251.04
Benítez, N., et al. 2004, ApJS, 150, 1
Bertin, E., & Arnouts, S. 1996, A&AS, 117, 393
Brotherton, M. S., Tran, H. D., Becker, R. H., Gregg, M. D., Laurent-Muehleisen, S. A., & White, R. L. 2001, ApJ, 546, 775
Brown, M. J. I., et al. 2006, ApJ, 638, 88
Bruzual, G., & Charlot, S. 2003, MNRAS, 344, 1000
Canalizo, G., & Stockton, A. 2001, ApJ, 555, 719
Cid Fernandes, R., Heckman, T., Schmitt, H., Delgado, R. M. G., & Storchi-Bergmann, T. 2001, ApJ, 558, 81
Conselice, C., Bershady, M., Dickinson, M., & Papuvich, C. 2003, AJ, 126, 1183
Cutri, R. M., Nelson, B. O., Kirkpatrick, J. D., Huchra, J. D., & Smith, P. J. 2001, in ASP Conf. Ser. 232, The New Era of Wide Field Astronomy, ed. R. G. Clowes, A. J. Adamson and, G. E. Bromage (San Francisco: ASP), 78
Dunlop, J. S., McLure, R. J., Kukula, M. J., Baum, S. A., O'Dea, C. P., & Hughes, D. H. 2003, MNRAS, 340, 1095
Eracleous, M., & Halpern, J. P. 1994, ApJS, 90, 1
Fanaroff, B. L, Riley, J. M. 1974, MNRAS, 167, 31P
Ferrarese, L., Merritt, D. 2000, ApJ, 539, 9
Fitzpatrick, E. L. 1999, PASP, 111, 63
Fitzpatrick, E. L., & Massa, D. 1990, ApJS, 72, 163
Floyd, D. J. E., Kukula, M. J., Dunlop, J. S., McLure, R. J., Miller, L., Percival, W. J., Baum, S. A., & O'Dea, C. P. 2004, MNRAS, 335, 196
Gebhardt, K., et al. 2000, ApJ, 539, L13
Gilli, R., Comastri, A., & Hasinger, G. 2007, A&A, 463, 79
Gilli, R., Salvati, M., & Hasinger, G. 2001, A&A, 366, 407
Glasser, G. J. 1962, J. American Stat. Assoc., 57, 648
Glikman, E., Gregg, M. D., Lacy, M., Helfand, D. J., Becker, R. H., & White, R. L. 2004, ApJ, 607, 60
Glikman, E., Helfand, D. J., White, R. L., Becker, R. H., Gregg, M. D., & Lacy, M. 2007, ApJ, 667, 673
Guyon, O., Sanders, D. B., & Stockton, A. N. 2006, ApJS, 166, 89
Heckman, T. M., Blitz, L., Wilson, A. S., Armus, L., & Miley, G. K. 1989, ApJ, 342, 735

Hopkins, P. F., Hernquist, L., Cox, J. C., Di Matteo, T., Robertson, B., & Springel, V. 2006, ApJS, 163, 1
Hopkins, P. F., Hernquist, L., Martini, P., Cox, T. J., Robertson, B., Di Matteo, T., & Springel, V. 2005, ApJ, 625, L71
Hopkins, P. F., Hernquist, L., Cox, T. J., & Keres, D. 2007a, ApJ, submitted (arXiv: 0706.1243)
Hopkins, P. F., Richards, G. T., & Hernquist, L. 2007b, ApJ, 654, 731
Hutchings, J. B., Cherniawsky, A., Cutri, R. M., & Nelson, B. O. 2006, AJ, 131, 680
Hutchings, J. B., Maddox, N., Cutri, R. M., & Nelson, B. O. 2003, AJ, 126, 63
Ilbert, O., et al. 2006, A&A, 453, 809
Komossa, S., Burwitz, V., Hasinger, G., Predehl, P., Kaastra, J. S., & Ikebe, Y. 2003, ApJ, 582, L15
Lacy, M., Gates, E. L., Ridgway, S. E., de Vries, W., Canalizo, G., Lloyd, J. P., & Graham, J. R. 2002, AJ, 124, 3023
Lacy, M., Petric, A. O., Sajina, A., Canalizo, G., Storrie-Lombardi, L. J., Armus, L., Fadda, D., & Marleau, F. R. 2007, AJ, 133, 186
Lacy, M., et al. 2004, ApJS, 154, 166
Li, Y., Hernquist, L., Robertson, B., Cox, T. J., Hopkins, P. F., Springel, V., Gao, L., Di Matteo, T., Zentner, A. R., Jenkins, A., & Yoshida, N. 2007, 665, 187
Lotz, J. M., Primack, J., & Madau, P. 2004, AJ, 128, 163
Magorrian, J., et al. 1998, AJ, 115, 2285
Maiolino, R., Marconi, A., Salvati, M., Risaliti, G., Severgini, P., Oliva, E., La Franca, F., & Vanzi, L. 2001, A&A, 365, 28
Marble, A. R., Hines, D. C., Schmidt, G. D., Smith, P. S., Surace, J. A., Armus, L., Cutri, R. M., & Nelson, B. O. 2003, ApJ, 590, 707
Martínez-Sansigre, A., Rawlings, S., Lacy, M., Fadda, D., Marleau, F. R., Simpson, C. Willott, C. J., & Jarvis, M. J. 2005, Nature, 436, 666
McLure, R. J., Dunlop, J. S., & Kukula, M. J. 2000, MNRAS, 318, 693
McLure, R. J., Kukula, M. J., Dunlop, J. S., Baum, S. a., O'Dea, C. P., & Hughs, D. H. 1999, MNRAS, 308, 377
Norman, C., et al. 2002, ApJ, 571, 2188
Petrosian, V. 1976, ApJ, 209, L1
Richards, G. T. 2003, AJ, 126, 1131
Sanders, D. B., & Mirabel, I. F. 1996, ARA&A, 34, 749
Sanders, D. B., Scoville, N. Z., Zensus, A., Soifer, B. T., Wilson, T. L., Zylka, R. & Steppe, H. 1989, A&A, 213, 5
Skrutskie, M. F., et al. 1995, BAAS, 187, 7507
Springel, V., Di Matteo, T., & Hernquist, L. 2005, MNRAS, 361, 776
Stern, D., et al. 2005, ApJ, 631, 163
Surace, J. A., Sanders, D. B., & Evans, A. S. 2001, AJ, 122, 2791
Tremaine, S., et al. 2002, ApJ, 122, 549
Ueda, Y., Akiyama, M., Ohta, K., & Miyaji, T. 2003, ApJ, 598, 886
Urrutia, T., Lacy, M., Gregg, M. D., & Becker, R. H. 2005, ApJ, 627, 75
White, R. L., Helfand, D. J., Becker, R. H., Gregg, M. D., Postman, M., Lauer, T. R., & Oegerle, W. 2003, AJ, 126, 706
White, R. L., Helfand, D. J., Becker, R. H., Glikman, E., & De Vries, W. 2007, ApJ, 654, 99
Zakamska, N. L., et al. 2006, AJ, 132, 1496